J. Am. Soc. Mass Spectrom. (2017)
DOI: 10.1007/s13361-017-1661-8

RESEARCH ARTICLE

Benchmark Comparison for a Multi-Processing Ion Mobility Calculator in the Free Molecular Regime

Vaibhav Shrivastav,[1] Minal Nahin,[1] Christopher J. Hogan,[2] Carlos Larriba-Andaluz[1]

[1]Department of Mechanical Engineering, IUPUI, Indianapolis, IN 46202, USA
[2]Department of Mechanical Engineering, University of Minnesota, Minneapolis, MN 55455, USA

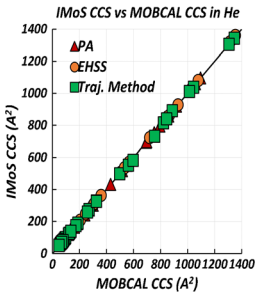

Abstract. A benchmark comparison between two ion mobility and collision cross-section (CCS) calculators, MOBCAL and IMoS, is presented here as a standard to test the efficiency and performance of both programs. Utilizing 47 organic ions, results are in excellent agreement between IMoS and MOBCAL in He and N_2, when both programs use identical input parameters. Due to a more efficiently written algorithm and to its parallelization, IMoS is able to calculate the same CCS (within 1%) with a speed around two orders of magnitude faster than its MOBCAL counterpart when seven cores are used. Due to the high computational cost of MOBCAL in N_2, reaching tens of thousands of seconds even for small ions, the comparison between IMoS and MOBCAL is stopped at 70 atoms. Large biomolecules (>10000 atoms) remain computationally expensive when IMoS is used in N_2 (even when employing 16 cores). Approximations such as diffuse trajectory methods (DHSS, TDHSS) with and without partial charges and projected area approximation corrections can be used to reduce the total computational time by several folds without hurting the accuracy of the solution. These latter methods can in principle be used with coarse-grained model structures and should yield acceptable CCS results.

Keywords: MOBCAL, IMoS, Mobility, CCS, Benchmark, Spectrometry, Trajectory method, EHSS, DHSS, TDHSS, Collision cross-section, Projection approximation

Received: 27 September 2016/Revised: 8 March 2017/Accepted: 14 March 2017

Introduction

Ion mobility spectrometry has become increasingly prevalent in analytical chemistry as well as aerosol science [1–9]. Aside from complementing mass spectrometry as an orthogonal technique [10–21], it is extensively used as a standalone instrument due to its portability and versatility [22–30]. Despite new advances in instrumentation, including improved resolution and transmission [26, 31–34], there has not been a parallel development in numerical calculation schemes for collision cross-sections and mobilities (i.e., the measured/inferred parameters in ion mobility spectrometry. Reasons behind such hindrance are 3-fold. The first problem is the difficulty that arises when trying to perform accurate calculations and the long associated times those numerical calculations take. The second problem has to do with the lack of well-established parameters, which are necessary for gas-phase calculations and which can only be obtained through careful experimental studies. The last problem is that there is a lack of reliable methods to perform gas-phase molecular dynamics; many of the existing forcefields are optimized to be used in solvents and therefore have limited use and accuracy in the gas phase. While we strive to improve every aspect of such numerical calculations, the purpose of this manuscript is to attempt to address the first of such problems, efficiency and performance, and additionally to characterize a range of possible methods to be used in the calculation of collision cross-sections. In this endeavor, we compare the CCS calculations using our in-house model, IMoS [35–39], with that of the most prominent existing method, MOBCAL [40, 41], while also incorporating new alternatives to reduce the computational costs. Although the IMoS and MOBCAL approach arise from a kinetic theory of gases, the methods follow rather different procedures. While MOBCAL enables calculation of the simplified first collision integral introduced by Mason and McDaniel [42], IMoS invokes a more general approach where gas molecule positions and velocities are directly calculated from a skewed Boltzmann

Electronic supplementary material The online version of this article (doi:10.1007/s13361-017-1661-8) contains supplementary material, which is available to authorized users.

Correspondence to: Carlos Larriba–Andaluz; *e-mail:* clarriba@iupui.edu

distribution [43–50]. Here we will show that both methods give very similar results, while the optimization, and importantly parallelization of IMoS makes it perform a few orders of magnitude faster. We also note there are other existing methods such as the projected superposition area (PSA) [51] algorithm; these are not included here due to the lack of available information in the literature on implementation to make a reasonable comparison.

The remainder of this manuscript is divided into two sections. The first introduces the similarities and differences between the two methods and also describes the interaction potentials used to compare both methods in two different gases, He and N_2. The second describes and compares the performance of both programs using the basic known algorithms: projected area approximation (PA), exact/elastic hard sphere scattering (EHSS), and trajectory method (TM). For larger molecules, where MOBCAL is extremely computationally expensive (due to its lack of parallelization), different trajectory methods in IMoS are compared and studied to find the most efficient and accurate algorithm.

Methods

Ion mobility spectrometry, as an analytical technique, is able to separate charged molecules (ions) or nanoclusters based on their drift velocity, v_{drift}, as they are driven by an electrical field, $\boldsymbol{E}$, through a carrier gas. Neglecting all perturbations and inertia and assuming that all directions are equally probable, the average electrical mobility at low speeds (relative to the mean thermal speed) can be inferred from the simple relation:

$$K\vec{E} = \vec{v}_{drift} \tag{1}$$

In general, however, the drift velocity is not known or easily calculated and the electrical mobility must be inferred by other means. To better define mobility, a useful expression is that of Mason-Schamp, given for ions and molecules in the free molecular regime [42]:

$$K = \left(\frac{\pi m_{red}}{8kT}\right)^{1/2} \frac{3ze}{4\rho_{gas}\Omega}, \tag{2}$$

where k is Boltzmann's constant, T is the background gas temperature, m_{red} is the reduced mass of the particles, z is the charge on the particle, ρ_{gas} is gas mass density, and Ω is the collision cross-section (CCS). The CCS is, succinctly, a term that quantifies the average effective area that interchanges momentum per unit time (force) with the buffer gas, when there is a velocity difference between an object and the gas it is immersed in. Its inference is by no means simple, and most calculation approaches, hence, utilize simplifications. Although there has been a fairly large amount of analytical attempts to calculate CCSs [43, 46–50, 52], the inherent difficulty associated mostly with parasitic effects, has led to the use of numerical methods to approximate these calculations. Noted in the introduction, two momentum transfer-based algorithms are compared here, the trajectory methods of IMoS and MOBCAL. Both methods employ relationships from the kinetic theory of gases, are loosely based on Onsager's [53, 54] reciprocal relations, and ultimately require the linearization of the gas molecule velocity distribution function proposed by Chapman and Enskog [55], which can only be employed for small perturbations and velocities. A brief description of both methods and the different potentials used is given below, with more detailed descriptions are provided in prior studies [38, 39, 47, 49, 55].

MOBCAL

MOBCAL's calculation method simplifies the collision cross-section by defining the momentum-transfer or diffusion cross-section integral, which is then averaged over all possible orientation and velocities [40, 42]:

$$\Omega_{avg}^{(1,1)} = \frac{1}{8\pi^2}\int_0^{2\pi} d\theta \int_0^{\pi} sin\phi d\phi \int_0^{2\pi} d\gamma \frac{\pi}{8}\left(\frac{\mu}{k_{BT}}\right)^3 \int_0^{\infty} g^5 e^{-\left(\frac{\mu g^2}{2k_{BT}}\right)} dg \int_0^{\infty} 2b(1-cos\chi)db \tag{3}$$

Here θ, ϕ, γ are the orientation angles, g is the relative velocity, b is the impact parameter, and χ is the deflection angle. If the deflection angle was known, CCSs could be easily calculated. In general, however, the deflection angle depends on the orientation angles, the velocity of gas molecules, the impact parameter, and the potential/collision interactions in the following manner [56, 57]:

$$\chi(\phi,\theta,\gamma,g,b) = \pi - 2b\int_{r_m}^{\infty} \frac{dr}{r^2\sqrt{1-\frac{b^2}{r^2}-\frac{\Phi(r)}{m_{red}g^2/2}}}, \tag{3'}$$

where r is the position of the gas molecule, r_m is the distance of closest approach, and $\Phi(r)$ is the potential interaction. Note that $r = r(x, y, z)$ will depend on the starting initial position and velocity of the gas molecule $(\phi, \theta, \gamma, g, b)$ as is reflected on the left-hand side of the equation. A depiction this mathematical relation is provided in Figure 1a. The deflection angle is not easily inferable and will, under most circumstances, require its numerical calculation. There also remain several simplifications in Equation 3. First, the velocity of the gas molecule is assumed much higher than that of the ion itself. A second assumption is that there is conservation of energy during

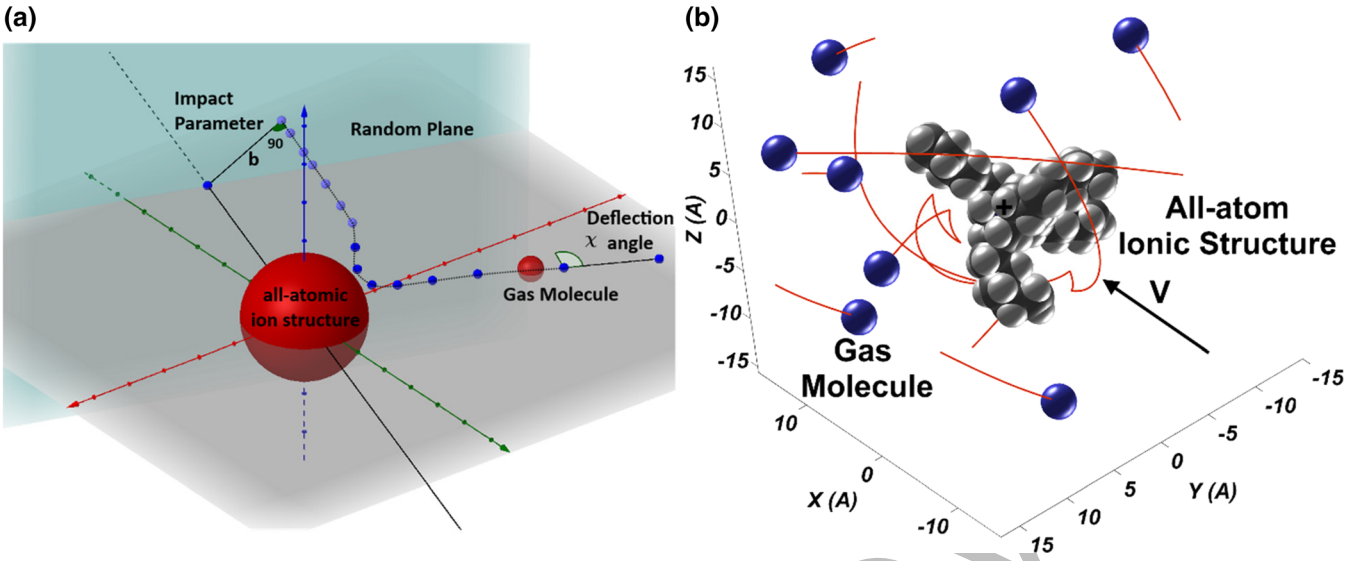

Figure 1. (**a**) Depiction of the process that MOBCAL undertakes to calculate the deflection angle of a gas molecule from a random plane orientation. (**b**) Depiction of IMoS control volume in which gas molecules enter from all directions

the collision as regarded by the fact that the only change in momentum transfer is given by the deflection angle χ. These are both reasonable assumptions under small values of E/N where N is the gas number density.

The numerical procedure in MOBCAL consists of randomly choosing a plane from which gas molecules at different impact parameters and velocities are emitted perpendicular to the plane. If there are potential interactions, the gas molecule paths may not be linear and trajectories are then followed using a time-step algorithm (4th order Runge–Kutta) until the gas molecule leaves the domain and the deflection angle χ recorded. The trajectories formed will therefore depend on the multiple potential interactions assumed to exist between the gas molecule and the atoms and location of the molecule charges. The Lennard-Jones parameters used must be optimized using experimental CCS [40, 41, 58–70].

IMoS

IMoS's algorithm principle is based on the general free molecular momentum transfer approach before Chapman and Enskog's simplification. The algorithm mimics a real gas environment based on a Maxwell-Boltzmann distribution that enters an enclosed control volume that travels with the ion's velocity $\boldsymbol{V}$. In order for this to happen, the control volume is chosen such that outside of it, the gas–ion potential interactions are considered to be negligible. The idea behind the algorithm, which is more commonly employed in continuum region drag calculations (i.e., in studying drag on macroscopic components), is to infer the position and velocity, both in angle and magnitude of gas molecules entering and exiting the domain so as to calculate the resulting momentum transfer. The velocity distribution of gas molecules entering the domain is given by [38, 39, 47]:

$$\rho = \frac{1}{h^3\pi^{3/2}}\exp\left(-\frac{\left\|\vec{c}_{gas}-\vec{V}^2\right\|}{h^2}\right) \tag{4}$$

Here, $\boldsymbol{c}$ is the velocity of the gas and $h = \left(\frac{2kT}{m_{gas}}\right)^{1/2}$ the most probable speed. The velocity distribution differs from the Maxwellian due to the consideration of the ion velocity $\boldsymbol{V}$. In such a case, the flow rate entering the control volume of area A is given by [49]:

$$Q = -\oint\int\int\int_{\boldsymbol{c}\cdot\boldsymbol{n}<0}\rho\left(\vec{c}\cdot\vec{n}\right)d^3c\,dA. \tag{5}$$

Here, $\boldsymbol{n}$ is the outward normal to the area element dA and $\boldsymbol{c}\cdot\boldsymbol{n} < 0$ is a global condition (not a limit of integration) that denotes that only gas molecules that are entering the domain are counted. The angle, velocity, and position of every gas molecule entering the control volume per unit time can, in principle, be extracted from Equation 5. A sketch of the method can be observed in Figure 1b. While IMoS could theoretically use the full expression for the distribution ρ in Equation 4, the low convergence rate and mathematical complexity precludes its use as long as the assumption of small E/N is in place. Instead, a linearization [39, 55] is employed in such cases where the ion velocity is small compared with the thermal gas velocity:

$$\rho = \frac{1}{h^3\pi^{3/2}}\exp\left(-\left(\vec{c}^{\,2}+\vec{V}^2-2\vec{c}\cdot\vec{V}\right)/h^2\right)\approx\rho_0 + 2\left(\vec{c}\cdot\vec{V}\right)\rho_0 = \rho_0+\rho_1, \tag{6}$$

where $\rho_0 = \frac{1}{h^3\pi^{3/2}}\exp(-c^2/h^2)$ is the general Maxwell Boltzmann distribution. Since the total momentum caused by ρ_0 is 0 (zero) by definition, Equation 5 can be simplified by using Equation 6:

$$Q = -\oint\int_{c\cdot n<0}\rho_1(\vec{c}\cdot\vec{n})d^3cdA = -\oint\int_{c\cdot n<0}2\left(\vec{c}\cdot\vec{V}\right)\rho_0(\vec{c}\cdot\vec{n})d^3cdA \quad (7)$$

In order to get the emission angles and velocities of the gas molecule, one must first choose the control volume. For instance, if a cuboid is chosen, the emission angles and velocities for the walls perpendicular to the bulk flow must obey the relationship:

$$\frac{K_1}{\pi^{3/2}h^5}\int_0^{\pi/2}\int_0^{2\pi}\int_0^{\infty}2V\ c^2cos^2(\theta)e^{-\left(c^2/h^2\right)}c^2\ sin(\theta)d\theta d\phi dc = 1 \quad (7')$$

which is separable in velocity and geometrical angles and where K_1 is a normalizing constant. Similarly, one can obtain the relation for other walls and cuboids.

Once the initial position, velocity, and angles of gas molecules are established, a Verlet algorithm is used to numerically follow the gas molecule through potential interactions with different atoms and charges until the gas molecule exits the domain. When this happens, the momentum transfer can be calculated from the difference in velocities and the mass of the gas. Note that IMoS allows for energy exchange to occur and therefore the deflection angle alone is not sufficient in general to calculate the momentum transfer per unit time. By assuming that all positions are equally probable, the averaged drag force (i.e., the momentum transfer per unit time) is related to the mobility and the collision cross-section through Equation 1:

$$Z(\Omega) = \frac{\overrightarrow{v}_{drift}}{<\overrightarrow{F_D}>} \quad (8)$$

The averaged drag force and average mobility obtained in Equation 8 has to be differentiated from the true mobility that can be obtained by using Happel and Brenner's method [71, 72].

Gas Molecule Trajectories

One can opt whether or not to include potential interactions between gas molecules and charges/atoms for both MOBCAL and IMoS. If only hard sphere potentials are considered, the trajectories are rectilinear and an instant reemission and change of velocity occurs upon collision of a gas molecule with one of the atoms. Collisions can happen a given number of times (multiple scattering) until the gas molecule leaves the domain. If the collisions are assumed to be specular and elastic, the method is referred to as exact/elastic hard sphere scattering or (EHSS) [41]. While the traditional implement of MOBCAL can only carryout specular elastic collisions with "frozen" ion structures, IMoS can also study inelastic and diffuse hard sphere collisions [4, 38, 39].These diffuse-inelastic type collisions seem to be much more prevalent larger mass gases (N_2 and Ar) at room temperature, and can be useful when studying large biomolecules, or even coarse grained model structures, for which interaction potentials with charges may be neglected. The method is then termed Diffuse Hard Sphere Scattering or DHSS.

If any other potential interactions (aside from hard sphere potentials) are taken into account, the method is regarded as a trajectory method (TM). Among the general possible potential interactions between ion and gas molecule, most notable are the Lennard-Jones potential interactions as well as the ion induced dipole potential. Both together can be written as [40, 70]:

$$\Phi(x,y,z) = 4\epsilon\sum_{i=1}^{n}\left[\left(\frac{\sigma}{r_i}\right)^{12} - \left(\frac{\sigma}{r_i}\right)^{6}\right] - \frac{\alpha}{2}\left(\frac{ze}{n}\right)^2\left[\left(\sum_{i=1}^{n}\frac{x_i}{r_i^3}\right)^2 + \left(\sum_{i=1}^{n}\frac{y_i}{r_i^3}\right)^2 + \left(\sum_{i=1}^{n}\frac{z_i}{r_i^3}\right)^2\right]$$

Here σ and ε are the inter-particle zero potential distance and the depth of the potential well, respectively, x_i, y_i, z_i, and r_i are the relative distances between the atoms (or charges) and the gas molecule, and α is the gas polarizability. IMoS and MOBCAL can take both interactions into account when using monoatomic gases such as He.

For diatomic nitrogen gas, a modification of the MOBCAL method was implemented to integrate the orientation of the molecule and ion-quadrupole potential. The quadrupole moment is obtained by placing one negative charge of 0.4825e on each nitrogen and one positive charge of 0.965e in the center of the molecule. In such a way, the quadrupole potential can be expressed as:[73, 74]

$$\Phi_{IQ}(x,y,z) = \sum_{j=1}^{3}\sum_{i=1}^{n}\frac{z_iz_je^2}{r_{ij}^3} \quad (10)$$

The index j denotes three different N_2 charges (where 2 is the center charge) and index i indicates the charges on the ion. The orientation of the N_2 molecule was taken into account by assuming an appropriate weighted impact parameter. While IMoS has its own way of taking into account the orientation of the diatomic gas molecule [35], it will not be pursued here since the purpose of this manuscript is to compare the results and performances of the two methods. Instead, the ion-quadrupole potential and the weighted gas molecule orientation have been added to the IMoS program.

IMoS has the option of choosing which potentials to use for each gas. One could for instance use hard sphere potentials together with ion-induced dipole potentials. For example, if the re-emission is assumed as diffuse and inelastic and the ion induced dipole potential is the only potential considered, the method is regarded as TDHSS where the T stands for trajectory calculation.

Algorithm Testing

Both numerical programs were tested on the same Intel i7 3.6Ghz chip with four physical cores. MOBCAL is not parallelized and it was run one instance at a time. IMoS can be parallelized (OMP) and was run once instance at a time with different number of threads (1, 5, and 7 threads). While a linear increase in speed is not expected when using hyperthreaded parallelization, the increase in speed between 5 and 7 threads is quite notable. We also note here that MOBCAL could be easily parallelized and a linear increase in speed would also be expected. When studying large biomolecules (>1000 atoms), MOBCAL was too inefficient to be used and only the parallelized version of IMoS was used on a Linux environment using a 2.8Ghz chip with 16 threads.

Finally, the structures studied herein (listed in the Supplementary Information) have been taken from literature and not all of them are optimized for the gas phase. As such, the CCSs that appear in this manuscript will not necessarily agree with experimentally measured CCSs; the structures simply serve to facilitate comparison between the two methods. Similar results that would be obtained in comparison were random structures chosen to validate the methods. Among the structures studied, supplementary information shows CCSs calculations for proteins (kindly provided by Iain Campuzano [70]), tetra-alkylammonium salts, fullerenes, ionic liquids, polyethylene glycol homo-polymer molecules, and proteins (kindly provided by Morgan Lawrentz and Iain Campuzano).

Results and Discussion

A cross-check of the results is obtained by comparing both programs in terms of efficiency and performance considering possible discrepancies, while trying to maintain equivalent parameters and potentials for each of the algorithms and for each gas examined. Simulations were run with the same number of gas molecules (or trajectories in the case of MOBCAL) for both programs; $9 \cdot 10^5$ molecules in He and $4 \cdot 10^5$ molecules in N_2. The uncertainty (~<0.1%) obtained when using such a large number of gas molecules is small enough that it can be obviated and was not studied here. The performance of each code was then tested by comparing MOBCAL to IMoS 1, 5, and 7 thread execution. When studying large molecules (>1000 atoms), different interaction approximations using different potentials were compared and interpreted in IMoS.

Figure 2a shows the calculated CCS comparison between MOBCAL and IMoS in He for three different methods, PA (projection approximation, which treats the CCS as equivalent to the orientationally averaged project area as was based on 2000 random orientations), EHSS, and the trajectory method. All three methods were employed to calculate the CCS of 47 different organic ions, including bioactive molecules, tetra-alkylammonium salts, fullerenes, ionic liquids, polyethylene glycol homo-polymer molecules, and proteins. To make PA and EHSS methods comparable for IMoS and MOBCAL, the same vdw radii were used for the sum of the atom and gas molecule (Supplementary Table S1b). For the TM method, the same Lennard-Jones potential parameters were used (Supplementary Table S1c). The temperature was kept constant at 301 K and the polarizability for the ion-induced dipole potential was chosen to be 0.2073 A^3. For a list of the molecules, vdw radii, and parameters used in the calculations, as well as for numerical results, we refer readers to Supplementary Table S1.

The resulting difference in CCS when using EHSS or PA is within <1%, and for most structures it is well below 0.1%. When testing trajectory methods, the calculated difference is slightly larger, but is still within 1%. This difference increased with fullerenes to 1.5% on average. The reason for such difference could not be pinpointed exactly, but it likely arises because of the inherent differences in the algorithms. IMoS considers collisions from all directions at every orientation with correctly distributed numbers of gas molecules entering the front and the back of the domain (more on the front). The relative velocities of the gas molecules from the front and the back are also slightly different (to account for the ion moving), which makes the trajectories different (See discussion in [39]). Finally, IMoS uses an adaptive time step (versus MOBCAL's constant time step) that minimizes errors by keeping the acceleration term from being too large. This becomes especially important close to large clusters of atoms and charges where the force term can become very large. In all, IMoS and MOBCAL treat trajectories differently and should yield slightly different results when using the same Lennard-Jones pairs. However, a small variation of the Lennard-Jones parameters (a factor of 1.015) in IMoS will yield values that are within 0.5% of those provided by MOBCAL for fullerenes.

Figure 2b shows the results when comparing CCS in N_2 for 16 different molecules. Only the TM method is shown as the comparison that the other two methods, PA and EHSS, would be intrinsically the same as in He. The trajectory method, conversely, now considers the ion-quadrupole potential provided in Equation 10, which dramatically increases the total

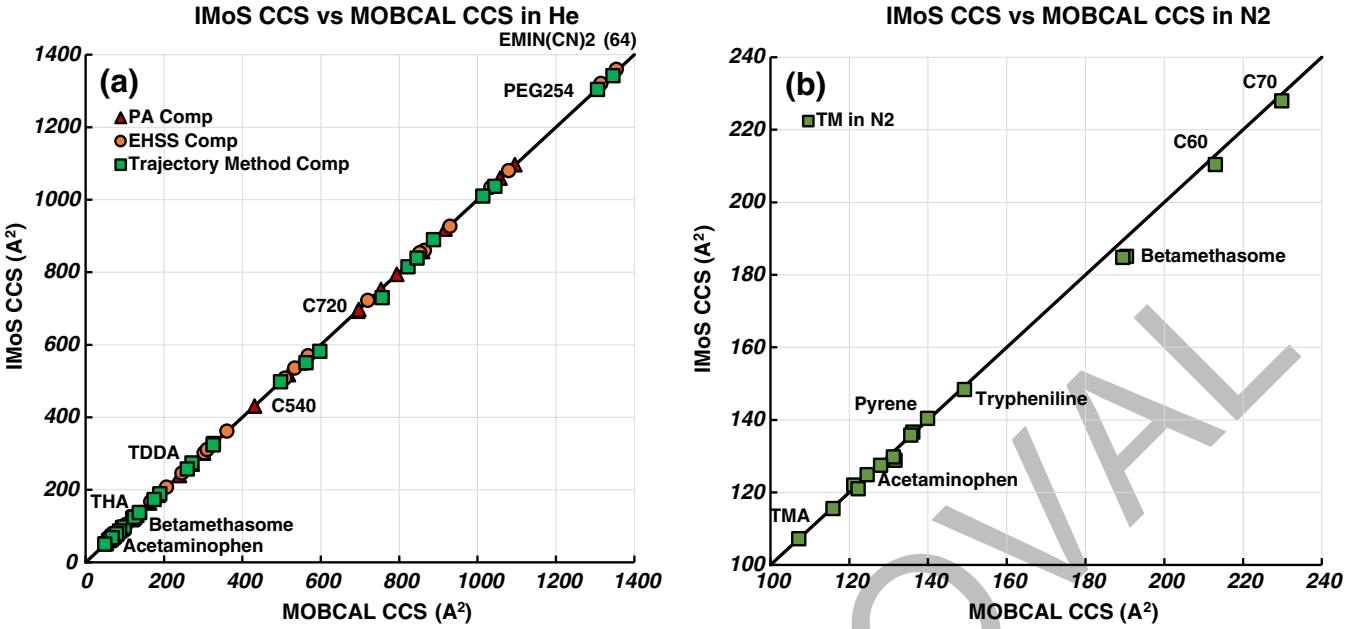

Figure 2. CCS calculation comparison between MOBCAL and IMoS for (**a**) PA, EHSS, TM in He, and (**b**) TM in N_2. TM in He incorporates Lennard-Jones and ion-induced dipole potentials whereas TM in N2 incorporates the potentials in He and ion quadrupole potential

computational time and precludes the study of molecules larger than 100 atoms for MOBCAL. The temperature during the calculation remained at 301 K while the polarizability used for N_2 is 1.7 A^3. Once again it is shown that the error difference between MOBCAL and IMoS is minimal; it is below 1% for most of the cases studied and slightly higher than 2% for only two of the molecules presented. Supplementary Table S2 shows a list of the numerical results and parameters used for the calculation in N_2. Although not attempted in this manuscript, a 4-6-12 potential with optimized Lennard-Jones parameters could be used alternatively to the ion quadrupole potential. These Lennard-Jones parameters would have to be optimized so that they also account for the ion-quadrupole potential. In this instance, the TM in N_2 is expected to be as computationally expensive as it is in He.

With demonstration that IMoS and MOBCAL agree quantitatively to a high degree, it is reasonable to test the performance of both methods. Since MOBCAL calculates all three methods simultaneously, PA, EHSS, and TM, an option was to not modify the algorithm and to compute the total completion time of the program. This option seemed reasonable since it benefits from not having to modify the code and because TM accounts for more than 90% of the total computational time in all cases studied. To make an acceptable comparison between IMoS and MOBCAL, IMoS was also run for the same three methods. Figure 3a shows the total completion time in He for IMoS and MOBCAL as a function of the number of atoms. The first thing to note is that the time for both methods increases approximately linearly with the number of atoms, although there is a minimum base cost that can be observed as the number of atoms gets lower. When comparing MOBCAL and IMoS on a 1:1 core ratio, IMoS is around one order of magnitude more efficient than MOBCAL. This can be increased to about two orders of magnitude when up to seven cores are used (on a four physical plus four virtual machine). The increase in speed per number of cores is not linear but significantly close. This linear increase can be explained by the fact that each gas molecule calculation is computed independently of each other, given that all calculations are performed in the free molecular regime, and can be easily parallelized. One can expect the difference to increase several-fold when 16 or 24 cores are used.

Figure 3b shows the total time as a function of the number of atoms when either MOBCAL or IMoS (only seven cores are shown) are used in diatomic nitrogen. As stated above, the addition of the ion-quadrupole potential significantly increases the computational time required, which becomes computationally burdensome when using MOBCAL. Despite the drop in speed, the linear dependence of time with the number of atoms can still be observed in both methods. While IMoS still requires approximately 100 s for the 70 atom structure, the computational time for MOBCAL is already in the tens of thousands of seconds for tens of atoms, precluding a reasonable comparison of both calculations for structures that are larger than a hundred atoms.

Although IMoS has the advantage of being parallelizable and providing trajectory method CCSs for structures of tens of thousands of atoms in modest time, doing full TM for large biomolecules (up to tens of thousands of atoms) remains computationally expensive and time-consuming, especially in the case of N_2. As molecules become larger, however, the interaction between gas molecules and each individual atom and/or

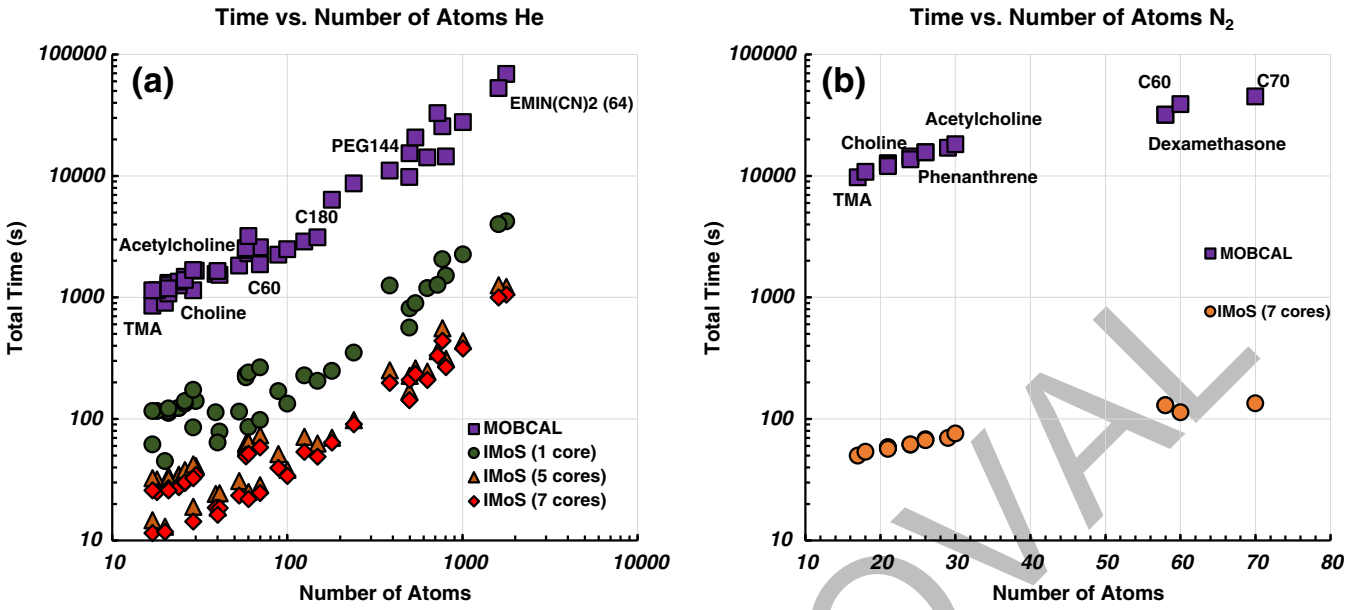

Figure 3. Total time to perform PA, EHSS, and TM methods as a function of the number of atoms for MOBCAL and IMoS (for 1, 5, and/or 7 cores) in (**a**) He, and (**b**) N_2

charge becomes less significant, particularly for atoms/charges that are far away, and can be substituted for a reasonable assumption. Although the assumption might differ from one gas to the other, there can be some simplifications that can lead to general corrections. This process can either be done by adding different contributions or by substituting these contributions for a more general parameter. Some of such simplifications are implemented in IMoS and will be tested and compared.

For example, EHSS is a simplification that is effective for CCS calculations in He. In He, the attractive component of the Lennard-Jones potential is small (very small well depth) and decays at the rate of $1/r^6$ as one moves far away from the atom while the repulsive component is still considerably large when the gas molecule collides with the atom. These two effects can be easily substituted by a slightly larger atom using hard sphere potentials. Another possible simplification could be to substitute the Trajectory Method for a simple Projected Area Algorithm since the algorithm seems to work well for small structures with values that are reasonably close to TM. Shown in Figure 4a is the ratio between TM and EHSS and TM and PA for several structures in He in the range of tens of thousands of atoms. Note that at large sizes, the PA by itself cannot yield good estimates while EHSS still remains an acceptable solution even at tens of thousands of atoms. The reason behind the observed difference lies in the scattering effect that occurs in larger structures and that is neglected in the projected area method. In general, using the EHSS method would therefore be much faster and perhaps just as precise as using the more sophisticated TM method for larger molecules. The sound agreement between EHSS and TM in He shown here is well known, and empirical and semi-empirical laws have been put in place to relate the two calculations [4, 35, 75].

While EHSS offers a good alternative to TM in He, it fails to give a good approximation in heavier gases such as N_2 or Ar even for the smallest of ions (although it seems to asymptotically converge to the TM CCS for clusters larger than 30,000 atoms) [4]. This is shown in Figure 4b for ions up to 70 atoms where the TM/EHSS ratio seems to yield high values close to 1.8 for the smallest structures and starts to drop towards a value between 1.25 and 1.5. The large difference observed for the smallest ions (up to 30 atoms) can be attributed to the ion-induced dipole potential. This potential rapidly decays and should only account to approximately 1% for the 70 atoms molecule (C70 fullerene) [39], where there remains an observable difference. This observed discrepancy in heavier gases can arguably be related to the re-emission of the impinging gas molecules being diffuse instead of specular (when considering frozen ion structures), as noted by Epstein in 1924 [46], precluding the possible use of EHSS in heavier gases [4, 38, 39]. The diffuse nature of the remission could either come from the physical action–reaction transfer caused by a much heavier atom (N versus He) on a vibrating atom, which could not directly be explained by the TM method since it does not consider translation/vibrations of atoms, or it could come from the effect of multiple Lennard-Jones potential wells (much stronger than in the case of He) of collision-adjacent atoms, which reorient the gas molecule in a non-specular direction. Whether it is an effect of physical momentum transfer or just a potential interaction or a mixture of both, an approximation could tentatively be proposed instead of the full trajectory method for larger ions. The most logical approximation that one can immediately apply is to consider the re-emission to be completely diffuse (DHSS) using a slightly modified velocity distribution. This modified distribution in IMoS is chosen in this case so as to match the constant value inferred by Millikan

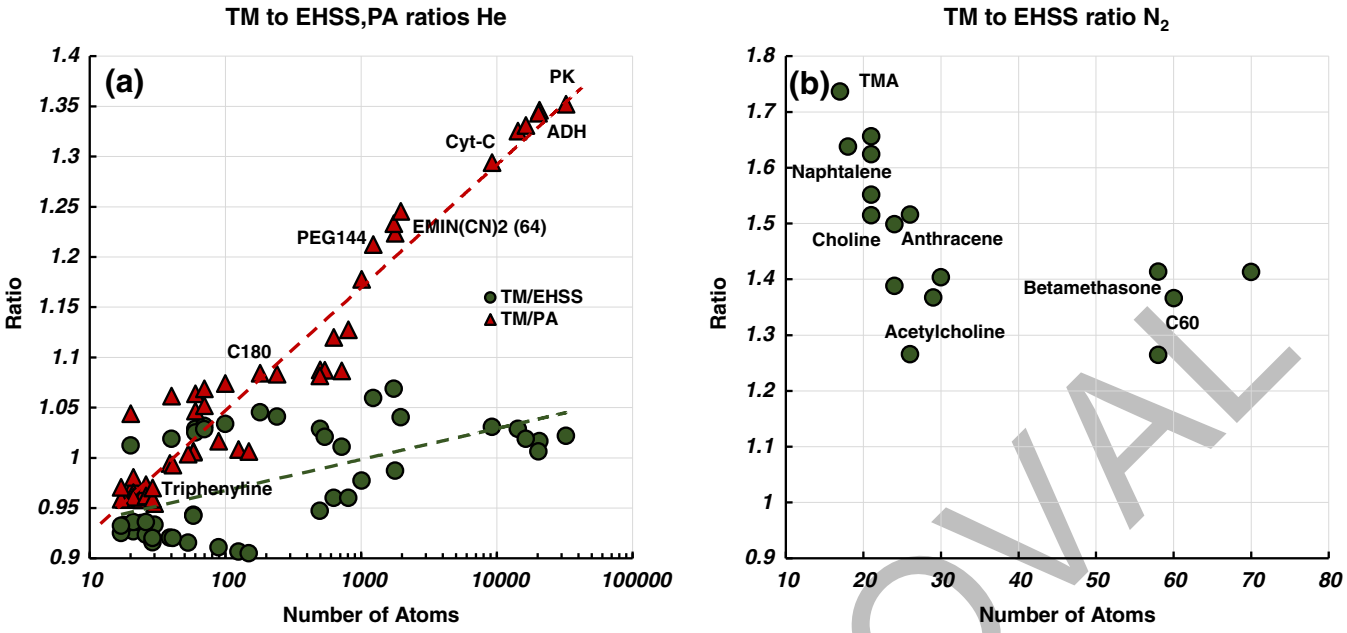

Figure 4. (**a**) Ratio of TM/EHSS (green circles) and TM/PA (red triangles) CCS versus the number of atoms in He, and (**b**) Ratio of TM/EHSS CCS as a function of the number of atoms in N_2

in his oil drop experiments of 1.36 [52]. This method benefits from not having to calculate the Lennard-Jones interaction between the gas molecule and atoms, significantly decreasing the number of operations at every iteration. Figure 5a shows the comparison between DHSS, DHSS accounting for the ion induced dipole potential (TDHSS) and TM for multiply charged ions. Given the large simplification, the agreement of the methods when the ion-induced dipole potential is included is quite remarkable, having errors of only a couple percent for most of the cases studied for a fairly large range of sizes.

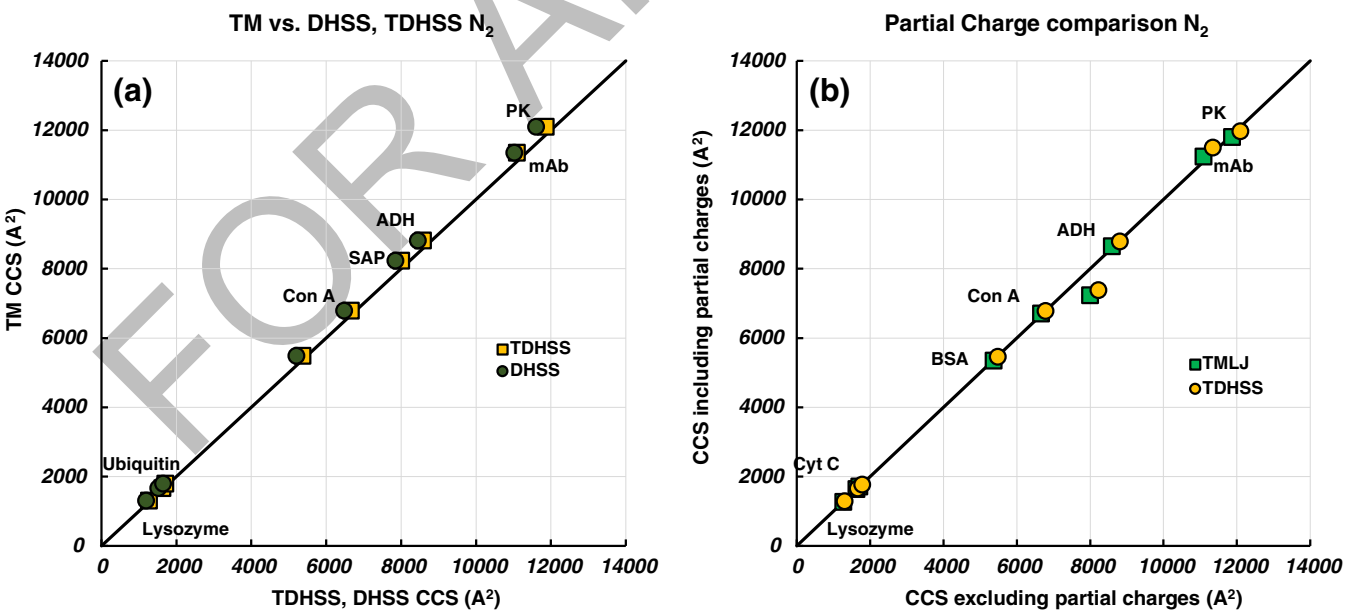

Figure 5. (**a**) Comparison of calculated CCS between TM and diffuse scattering methods with (TDHSS, yellow squares) and without (DHSS, green circles) ion-induced dipole potential for multiply charged relatively large molecules (>1000 atoms) in N_2. (**b**) Comparison between assigning partial charges and centering the absolute value of the charge in the center or specific ions. This comparison is performed for the regular TM method (TMLJ) and for the diffuse scattering trajectory Method (TDHSS)

Additional computational cost derives from calculating the ion-induced dipole potential between partial charges in every atom and the corresponding gas molecule. Since the interaction potentials decay extremely fast as one gets far from the center of the atom and given that all directions are equally probable (small dipole effects will cancel out), another approximation for large molecules is to locate the overall charge value either only on the center of the molecule (if possible) or on the appropriate charge carriers, leaving the rest of the atoms neutral. Figure 5b shows the difference in CCS between applying partial charges (taken from Amber forcefield) or applying the charges directly in the center for large biomolecules. As expected, the error associated with not applying partial charges to the atoms is negligible (<2%) for such large molecules.

Figure 6 shows the time comparison for the TM (not using ion-quadrupole potential) and TDHSS methods with and without charges using 16 cores. For such large entities, the effect of the ion quadrupole is minimal but increases the calculation by an order of magnitude and was excluded from these calculations. Note that the choice of TDHSS without partial charges reduces the total time by a factor of 30 without incurring in a large error. This is very significant for protein kinase (PK protein) where the time is reduced from several hours to around 15 min.

While this simplification is substantial, ideally one can simplify the calculations even more if there were a simple way to infer the contribution of the ion induced dipole potential and the enhancement due to scattering. If these were known, one could infer the CCS by just calculating the average projected area and adding the contributions. For example, the CCS could be given by [38, 39]:

$$\Omega = L\,\xi PA \tag{11}$$

where L is a correction factor to take into account the ion induced dipole potential and ξ is the reemission enhancement. The reemission enhancement, otherwise known as accommodation coefficient, is known to be constant and close to 1.36 in the case of nitrogen [52] but needs to be experimentally derived for He. Shown elsewhere [38, 39] and in good agreement with calculations reported by Mason and McDaniel, L can be approximated for a sphere in N_2 by the equation:

$$L \simeq \left[1 + A\varphi_e\left(1 + \frac{1}{\xi}\left(\frac{5}{22} + \frac{5}{7}\varphi_e\right)\right)\right] \text{ if } \varphi_e \leq 1 \tag{12}$$

where $A = (1/5, 3/5)$ is a numerically derived parameter selected to be 2/5 here, ξ is chosen to be 1.36, and $\varphi_e = U_{pol}\left(\frac{d_p+d_g}{2}\right)/kT$ denotes the polarization potential $U_{pol} = \frac{\alpha z^2 e^2}{8\pi\epsilon\epsilon_0 r_i^4}$ evaluated at the surface $r_i=(d_p+ d_g)/2$ assuming that all charges are in the center. In the case of non-spherical particles, $(d_p+ d_g)/2$ can be approximated by the value $(PA/\pi)^{1/2}$ as long as the atom structure does not deviate too much from a globule. This semi-empirical equation is formed by a correction due to direct impingement of molecules plus a correction due to grazing molecules (those inside the factor $1/\xi$) that do not directly impinge but still transfer momentum. Figure 7 shows the comparison between the TM method and the approximation in Equation 11 for N_2. This simplification works remarkably well at room temperature and should hold for small changes in temperature. When the projected area correction is employed, the total time taken to perform calculations of structures over 10,000 atoms is of only a few s.

Finally, needless to say, many of these simplifications will also work with coarse grained molecules due to the fact that

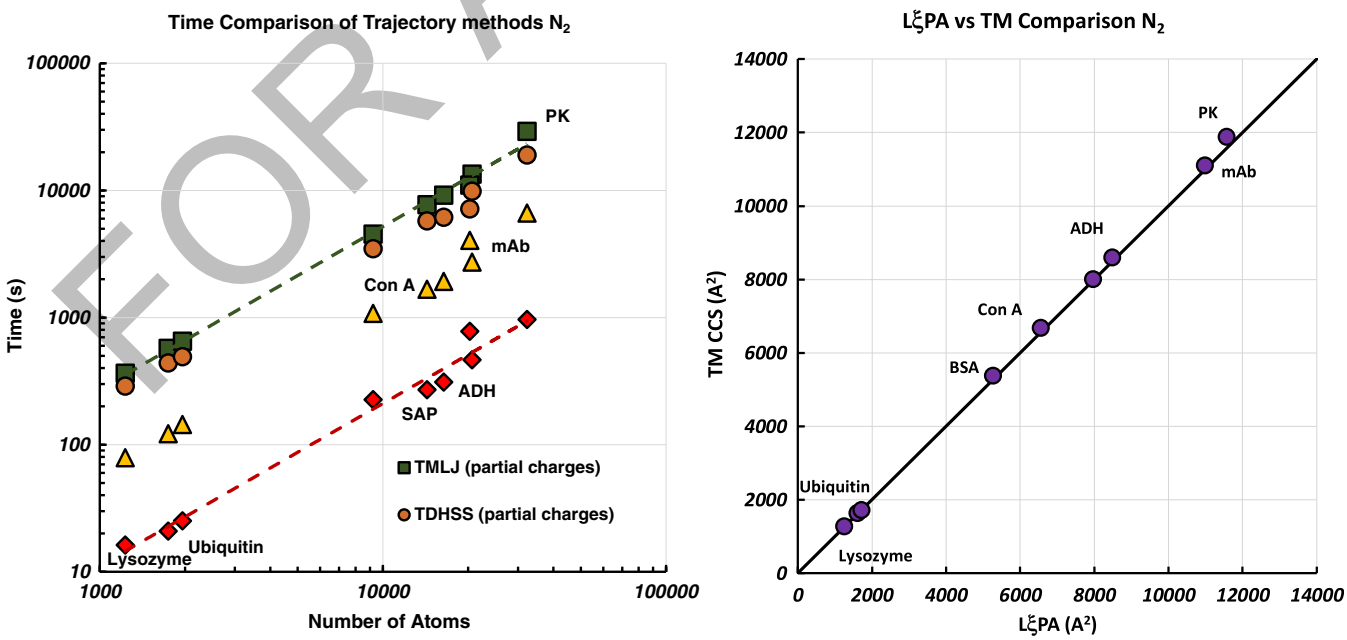

Figure 6. Time comparison between different approximations of trajectory methods as a function of the number of atoms

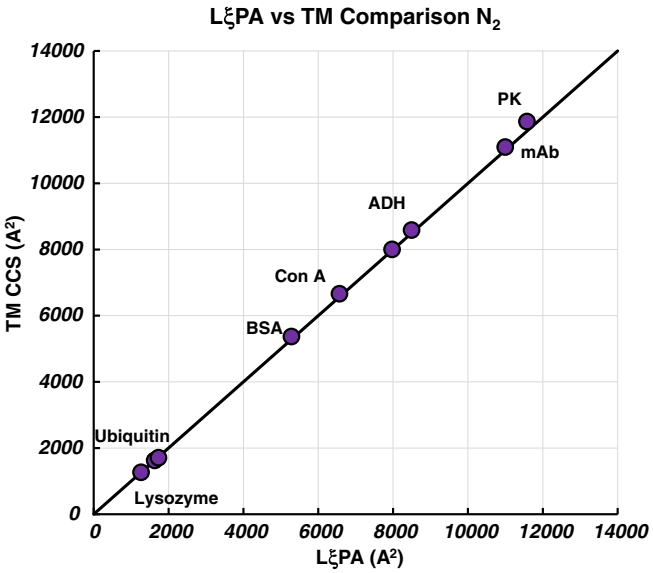

Figure 7. Relation between the theoretical approximation LξPA and the TM method using the correction from Equation 11

most of the simplifications applied inherently adapt to coarse grained model structures [76]. TDHSS without partial charges or the simplification used in Equation 12 should yield very similar results whether applied to an all-atomic structure or to a simplification of the same structure using only approximations of major components.

Conclusions

A benchmark comparison between different algorithms has been performed to compare efficiency and performance of existing numerical algorithms and their simplifications. The following conclusions can be extracted from the study:

1) IMoS and MOBCAL are inherently different numerical programs. Nonetheless, when Chapman-Enskog simplifications are performed with IMoS, the CCS results between the two algorithms are comparable.
2) IMoS and MOBCAL yield very similar results (in general <1% difference) when the same conditions are applied for the compounds studied herein and for all methods studied: PA, EHSS, and TM with and without ion-quadrupole potentials for He and N_2, respectively. Note that given that both methods have a different approach, this agreement only strengthens the validity of both programs and the approximations used.
3) Using the same number of gas molecules, IMoS is about one order of magnitude more efficient than MOBCAL in all the cases studied.
4) IMoS can be parallelized and its increase in speed is close to linear with the number of processors.
5) When large biomolecules need to be studied, the algorithms are not nearly efficient enough even when 16 processors are used. Therefore, simplifications of the algorithms are proposed.
6) Simplifications of He include the EHSS algorithm, which seems to be very suitable for large biomolecules due to its simplicity, its efficiency, and its reckoning of the scattering. Simplifications done in N_2 include the TDHSS model for structures larger than 200 atoms with and without partial charges and the correction to the projected area used in Equation 11.
7) Simplifications used in N_2 could be extrapolated to coarse grained models because of its inherent simplification of collisions and potentials.

This study is only meant as a comparison between existing algorithms to calculate CCS and to attest their validity. MOBCAL could most likely be written as efficiently as IMoS and the comparison in speed between the two methods only serves the purpose of showing how efficiency and suitable approximations can decrease the total computational time several orders of magnitude.

Supplemental Information

A list with the numerical results from the computations, the relative accuracy, speed and parameters used have been added to the supplementary information. An output of the IMoS software has also been added. An executable of IMoS is available from www.imospedia.com.

References

1. Bohrer, B.C., Mererbloom, S.I., Koeniger, S.L., Hilderbrand, A.E., Clemmer, D.E.: Biomolecule analysis by ion mobility spectrometry. Annu. Rev. Anal. Chem. **1**, 293–327 (2008)
2. Larriba, C., de la Mora, J.F.: The gas phase structure of coulombically stretched polyethylene glycol ions. J. Phys. Chem. B **116**, 593–598 (2012)
3. Larriba, C., Hogan, C.J., Attoui, M., Borrajo, R., Garcia, J.F., de la Mora, J.F.: The mobility-volume relationship below 3.0 nm examined by tandem mobility-mass measurement. Aerosol. Sci. Tech. **45**, 453–467 (2011)
4. Larriba-Andaluz, C., Fernandez-Garcia, J., Ewing, M.A., Hogan, C.J., Clemmer, D.E.: Gas molecule scattering and ion mobility measurements for organic macro-ions in He versus N-2 environments. Phys. Chem. Chem. Phys. **17**, 15019–15029 (2015)
5. Li, M.D., Mulholland, G.W., Zachariah, M.R.: Understanding the mobility of nonspherical particles in the free molecular regime. Phys. Rev. E **89**, 029905 (2014)
6. Oberreit, D., Rawat, V.K., Larriba-Andaluz, C., Ouyang, H., McMurry, P.H., Hogan, C.J.: Analysis of heterogeneous water vapor uptake by metal iodide cluster ions via differential mobility analysis-mass spectrometry. J. Chem. Phys. **143**,104204 (2015)
7. Ruotolo, B.T., Benesch, J.L.P., Sandercock, A.M., Hyung, S.J., Robinson, C.V.: Ion mobility-mass spectrometry analysis of large protein complexes. Nat. Protoc. **3**, 1139–1152 (2008)
8. Trimpin, S., Clemmer, D.E.: Ion mobility spectrometry/mass spectrometry snapshots for assessing the molecular compositions of complex polymeric systems. Anal. Chem. **80**, 9073–9083 (2008)
9. Zhang, C.L., Thajudeen, T., Larriba, C., Schwartzentruber, T.E., Hogan, C.J.: Determination of the scalar friction factor for nonspherical particles

and aggregates across the entire Knudsen number range by direct simulation Monte Carlo (DSMC). Aerosol. Sci. Tech. **46**, 1065–1078 (2012)
10. Clemmer, D.E., Pierson, N., Shi, H.L., Ewing, M.: Developing IMS-MS techniques as a means of following structural transitions of biopolymers in solution. Abstract Paper Am. Chem. S **247**, (2014)
11. Criado-Hidalgo, E., Fernandez-Garcia, J., de la Mora, J.F.: Mass and charge distribution analysis in negative electrosprays of large polyethylene glycol chains by ion mobility mass spectrometry. Anal. Chem. **85**, 2710–2716 (2013)
12. Ewing, M.A., Glover, M.S., Clemmer, D.E.: Hybrid ion mobility and mass spectrometry as a separation tool. J. Chromatogr. A **1439**, 3–25 (2016)
13. Fenn, L.S., McLean, J.A.: Simultaneous glycoproteomics on the basis of structure using ion mobility-mass spectrometry. Mol. Biosyst. **5**, 1298–1302 (2009)
14. Fernandez-Garcia, J., de la Mora, J.F.: Measuring the effect of ion-induced drift-gas polarization on the electrical mobilities of multiply-charged ionic liquid nanodrops in air. J. Am. Soc. Mass Spectrom. **24**, 1872–1889 (2013)
15. Gaye, M.M., Nagy, G., Clemmer, D.E., Pohl, N.L.B.: Multidimensional analysis of 16 glucose isomers by ion mobility spectrometry. Anal. Chem. **88**, 2335–2344 (2016)
16. Glover, M.S., Dilger, J.M., Acton, M.D., Arnold, R.J., Radivojac, P., Clemmer, D.E.: Examining the influence of phosphorylation on peptide ion structure by ion mobility spectrometry-mass spectrometry. J. Am. Soc. Mass Spectrom. **27**, 786–794 (2016)
17. Larriba, C., de la Mora, J.F., Clemmer, D.E.: Electrospray ionization mechanisms for large polyethylene glycol chains studied through tandem ion mobility spectrometry. J. Am. Soc. Mass Spectrom. **25**, 1332–1345 (2014)
18. Matz, L.M., Hill, H.H.: Evaluating the separation of amphetamines by electrospray ionization ion mobility spectrometry/MS and charge competition within the ESI process. Anal. Chem. **74**, 420–427 (2002)
19. McLean, J.A.: The mass-mobility correlation redux: the conformational landscape of anhydrous biomolecules. J. Am. Soc. Mass Spectrom. **20**, 1775–1781 (2009)
20. Trimpin, S., Tan, B., Bohrer, B.C., O'Dell, D.K., Merenbloom, S.I., Pazos, M.X., Clemmer, D.E., Walker, J.M.: Profiling of phospholipids and related lipid structures using multidimensional ion mobility spectrometry-mass spectrometry. Int. J. Mass Spectrom. **287**, 58–69 (2009)
21. Valentine, S.J., Kurulugama, R.T., Bohrer, B.C., Merenbloom, S.I., Sowell, R.A., Mechref, Y., Clemmer, D.E.: Developing IMS-IMS-MS for rapid characterization of abundant proteins in human plasma. Int. J. Mass Spectrom. **283**, 149–160 (2009)
22. Martinez-Lozano, P., Labowsky, M.: An experimental and numerical study of a miniature high resolution isopotential DMA. J. Aerosol Sci. **40**, 451–462 (2009)
23. Kumar, A., Kang, S., Larriba-Andaluz, C., Ouyang, H., Hogan, C.J., Sankaran, R.M.: Ligand-free Ni nanocluster formation at atmospheric pressure via rapid quenching in a microplasma process. Nanotechnology **25**, 385601 (2014)
24. Graves, B., Olfert, J., Patychuk, B., Dastanpour, R., Rogak, S.: Characterization of particulate matter morphology and volatility from a compression-ignition natural-gas direct-injection engine. Aerosol Sci. Tech. **49**, 589–598 (2015)
25. Flagan, R.C.: Continuous-flow differential mobility analysis of nanoparticles and biomolecules. Annu. Rev. Chem. Biomol. **5**, 255–279 (2014)
26. Eiceman, G.A., Krylov, E.V., Nazarov, E.G., Miller, R.A.: Separation of ions from explosives in differential mobility spectrometry by vapor-modified drift gas. Anal. Chem. **76**, 4937–4944 (2004)
27. Eiceman, G.A., Feng, Y.: Limits of separation of a multi-capillary column with mixtures of volatile organic compounds for a flame ionization detector and a differential mobility detector. J. Chromatogr. A **1216**, 985–993 (2009)
28. Carbone, F., Beretta, F., D'Anna, A.: Size distribution functions of ultrafine ashes from pulverized coal combustion. Combust. Sci. Technol. **182**, 668–682 (2010)
29. Carbone, F., Attoui, M., Gomez, A.: Challenges of measuring nascent soot in flames as evidenced by high-resolution differential mobility analysis. Aeroso l Sci. Tech. **50**, 740–757 (2016)
30. Attoui, M., de la Mora, J.F.: Flow driven transmission of charged particles against an axial field in antistatic tubes at the sample outlet of a differential mobility analyzer. J. Aerosol Sci. **100**, 91–96 (2016)
31. Webb, I.K., Garimella, S.V.B., Norheim, R.V., Baker, E.S., Ibrahim, Y.M., Smith, R.D.: A structures for lossless ion manipulations (SLIM) module for collision induced dissociation. J. Am. Soc. Mass Spectrom. **27**, 1285–1288 (2016)
32. Ridgeway, M.E., Kaplan, D.A., Park, M.A.: Trapped ion mobility spectrometry. Abstract Paper Am. Chem. S **244**, (2012)
33. Fernandez-Lima, F.A., Kaplan, D.A., Park, M.A.: Note: integration of trapped ion mobility spectrometry with mass spectrometry. Rev. Sci. Instrum. **82**, 126106 (2011)
34. Chen, T.C., Ibrahim, Y.M., Webb, I.K., Garimella, S.V.B., Zhang, X., Hamid, A.M., Deng, L.L., Karnesky, W.E., Prost, S.A., Sandoval, J.A., Norheim, R.V., Anderson, G.A., Tolmachev, A.V., Baker, E.S., Smith, R.D.: Mobility-selected ion trapping and enrichment using structures for lossless ion manipulations. Anal. Chem. **88**, 1728–1733 (2016)
35. Larriba-Andaluz, C., Hogan, C.J.: Collision cross -ection calculations for polyatomic ions considering rotating diatomic/linear gas molecules. J. Chem. Phys. **141**, 194107 (2014)
36. Ouyang, H., Larriba-Andaluz, C., Oberreit, D.R., Hogan, C.J.: The collision cross-sections of iodide salt cluster ions in air via differential mobility analysis-mass spectrometry. J. Am. Soc. Mass Spectrom. **24**, 1833–1847 (2013)
37. Larriba-Andaluz, C., Hogan, C.: Novel interfaced approach to mobility calculations with diffuse scattering and Maxwell rotational distributions for diatomic gases in the free molecular regime. Abstract Paper Am. Chem. S **246**, (2013)
38. Larriba, C., Hogan, C.J.: Ion mobilities in diatomic gases: measurement versus prediction with non-specular scattering models. J. Phys. Chem. A **117**, 3887–3901 (2013)
39. Larriba, C., Hogan, C.J.: Free molecular collision cross section calculation methods for nanoparticles and complex ions with energy accommodation. J. Comput. Phys. **251**, 344–363 (2013)
40. Mesleh, M.F., Hunter, J.M., Shvartsburg, A.A., Schatz, G.C., Jarrold, M.F.: Structural information from ion mobility measurements: effects of the long-range potential (vol 100, pg 16082, 1996). J. Phys. Chem. A **101**, 968–968 (1997)
41. Shvartsburg, A.A., Jarrold, M.F.: An exact hard-spheres scattering model for the mobilities of polyatomic ions. Chem. Phys. Lett. **261**, 86–91 (1996)
42. Mason, E.A., McDaniel, E.W. John Wiley and Sons: New York (1988)
43. Chan, P., Dahneke, B.: Free-molecule drag on straight chains of uniform spheres. J. Appl. Phys. **52**, 3106–3110 (1981)
44. Dahneke, B.E.: Slip correction factors for nonspherical bodies—I. introduction and continuum flow. J. Aerosol Sci. **4**, 139–145 (1973)
45. Dahneke, B.E.: Slip correction factors for nonspherical bodies—II. free molecule flow. J. Aerosol Sci. **4**, 147–161 (1973)
46. Epstein, P.S.: On the resistance experienced by spheres in their motion through gases. Phys. Rev. **23**, 710 (1924)
47. Garcia-Ybarra, P.L., Castillo, J.L., Rosner, D.E.: Drag on a large spherical aggregate with self-similar structure: an asymptotic analysis. J. Aerosol Sci. **37**, 413–428 (2006)
48. Mackowski, D.W.: Calculation of total cross-sections of multiple-sphere clusters. J. Opt. Soc. Am. A **11**, 2851–2861 (1994)
49. Mackowski, D.W.: Monte Carlo simulation of hydrodynamic drag and thermophoresis of fractal aggregates of spheres in the free-molecule flow regime. J. Aerosol Sci. **37**, 242–259 (2006)
50. de la Mora, J.F.: Free-molecule mobility of polyhedra and other convex hard-bodies. J. Aerosol Sci. **33**, 477–489 (2002)
51. Bleiholder, C., Wyttenbach, T., Bowers, M.T.: A novel projection approximation algorithm for the fast and accurate computation of molecular collision cross-sections. (I) method. Int. J. Mass Spectrom. **308**, 1–10 (2011)
52. Millikan, R.A.: The general law of fall of a small spherical body through a gas, and its bearing upon the nature of molecular reflection from surfaces. Phys. Rev. **22**, 1–23 (1923)
53. Onsager, L.: Reciprocal relations in irreversible processes. I. Phys. Rev. **37**, 405 (1931)
54. Onsager, L.: Reciprocal relations in irreversible processes. II. Phy. Rev. **38**, 2265 (1931)
55. Chapman, S., Cowling, T.G. Cambridge University Press: (1970)
56. Li, Z.G., Wang, H.: Drag force, diffusion coefficient, and electric mobility of small particles. II. Appl. Phys. Rev. E **68**, 061207 (2003)
57. Li, Z.G., Wang, H.: Drag force, diffusion coefficient, and electric mobility of small particles. I. Theory applicable to the free-molecule regime. Phys. Rev. E **68**, 061206 (2003)

58. Clemmer, D.E., Jarrold, M.F.: Ion mobility measurements and their applications to clusters and biomolecules. J. Mass Spectrom. **32**, 577–592 (1997)
59. Dugourd, P., Hudgins, R.R., Clemmer, D.E., Jarrold, M.F.: High-resolution ion mobility measurements. Rev. Sci. Instrum. **68**, 1122–1129 (1997)
60. Dugourd, P., Hudgins, R.R., Jarrold, M.F.: High-resolution ion mobility studies of sodium chloride nanocrystals. Chem. Phys. Lett. **267**, 186–192 (1997)
61. Hudgins, R.R., Dugourd, P., Tenenbaum, J.M., Jarrold, M.F.: Structural transitions in sodium chloride nanocrystals. Phys. Rev. Lett. **78**, 4213–4216 (1997)
62. Hudgins, R.R., Woenckhaus, J., Jarrold, M.F.: High resolution ion mobility measurements for gas phase proteins: correlation between solution phase and gas phase conformations. Int. J. Mass Spectrom. **165**, 497–507 (1997)
63. Mesleh, M.F., Hunter, J.M., Shvartsburg, A.A., Schatz, G.C., Jarrold, M.F.: Structural information from ion mobility measurements: effects of the long-range potential. J. Phys. Chem.-US **100**, 16082–16086 (1996)
64. Shelimov, K.B., Clemmer, D.E., Hudgins, R.R., Jarrold, M.F.: Protein structure in vacuo: gas-phase conformations of BPTI and cytochrome *c*. J. Am. Chem. Soc. **119**, 2240–2248 (1997)
65. Shelimov, K.B., Jarrold, M.F.: "Denaturation" and refolding of cytochrome *c* in vacuo. J. Am. Chem. Soc. **118**, 10313–10314 (1996)
66. Shelimov, K.B., Jarrold, M.F.: Conformations, unfolding, and refolding of apomyoglobin in vacuum: an activation barrier for gas-phase protein folding. J. Am. Chem. Soc. **119**, 2987–2994 (1997)
67 Shvartsburg, A.A., Hudgins, R.R., Dugourd, P., Jarrold, M.F.: Structural elucidation of fullerene dimers by high-resolution ion mobility measurements and trajectory calculation simulations. J. Phys. Chem. A **101**, 1684–1688 (1997)
68 Shvartsburg, A.A., Schatz, G.C., Jarrold, M.F.: Mobilities of carbon cluster ions: critical importance of the molecular attractive potential. J. Chem. Phys. **108**, 2416–2423 (1998)
69 Woenckhaus, J., Mao, Y., Jarrold, M.F.: Hydration of gas phase proteins: folded +5 and unfolded +7 charge states of cytochrome *c*. J. Phys. Chem. B **101**, 847–851 (1997)
70 Campuzano, I., Bush, M.F., Robinson, C.V., Beaumont, C., Richardson, K., Kim, H., Kim, H.I.: Structural characterization of drug-like compounds by ion mobility mass spectrometry: comparison of theoretical and experimentally derived nitrogen collision cross-sections. Anal. Chem. **84**, 1026–1033 (2012)
71 Happel, J., Brenner, H.: Springer: Netherlands, Dordrecht (1981)
72 Landau, L.D., Lifshitz, E.M. Pergamon Press: Oxford, England, New York (1987)
73 Kim, H.I., Kim, H., Pang, E.S., Ryu, E.K., Beegle, L.W., Loo, J.A., Goddard, W.A., Kanik, I.: Structural characterization of unsaturated phosphatidylcholines using traveling wave ion mobility spectrometry. Anal. Chem. **81**, 8289–8297 (2009)
74 Kim, H., Kim, H.I., Johnson, P.V., Beegle, L.W., Beauchamp, J.L., Goddard, W.A., Kanik, I.: Experimental and theoretical investigation into the correlation between mass and ion mobility for choline and other ammonium cations in N-2. Anal. Chem. **80**, 1928–1936 (2008)
75 Kinnear, B.S., Kaleta, D.T., Kohtani, M., Hudgins, R.R., Jarrold, M.F.: Conformations of unsolvated valine-based peptides. J. Am. Chem. Soc. **122**, 9243–9256 (2000)
76 Konijnenberg, A., Yilmaz, D., Ingolfsson, H.I., Dimitrova, A., Marrink, S.J., Li, Z.L., Venien-Bryan, C., Sobott, F., Kocer, A.: Global structural changes of an ion channel during its gating are followed by ion mobility mass spectrometry. Proc. Natl. Acad. Sci. U. S. A. **111**, 17170–17175 (2014)